ELSEVIER

Water reservoir loading of long anisotropic valleys with irregular topographies

Ernian Pan and Bernard Amadei

University of Colorado, Dept. of Civil Engineering, Boulder, CO

The nature of the stress field induced by water reservoir loading of long anisotropic valleys is considered using an analytical method proposed earlier by the authors. The rock mass is modeled as a linearly elastic, transversely isotropic or nearly isotropic and homogeneous continuum that deforms under a condition of plane strain. The method is used to determine stresses in symmetric and asymmetric valleys induced by water reservoir loading with or without gravity. Numerical examples are presented to analyze the disturbance associated with a water reservoir on the existing gravitational stress field. They show that the presence of a water reservoir does not much affect the horizontal and vertical gravity-induced normal stresses except near the valley bottom. There the effect of the water reservoir is to reduce the magnitude of the gravity-induced horizontal tensile stress and to increase the magnitude of the gravity-induced vertical compressive stress. On the other hand water reservoir loading affects the gravity-induced shear stress in a relatively large region below the valley. Finally a parametric study is presented on the effect of (1) water reservoir height, (2) degree of anisotropy, and (3) orientation of anisotropy on the magnitude and distribution of stresses induced by water reservoir loading only. © 1996 by Elsevier Science Inc.

Keywords: anisotropic elasticity, topography, conformal mapping, water reservoir loading

1. Introduction

Surface loading of a half space has long been a topic of interest in both pure and applied mechanics. Boussinesq was the first to drive an elastic solution for the stresses in a flat and isotropic half space subjected to surface point loads.[1] Conway and Ithaca[2,3] then extended this solution to the corresponding orthotropic case where the planes of elastic symmetry are either normal or inclined to the flat surface. Urena et al.[4] and Piquer et al.[5] obtained analytical solutions for the stresses in a transversely isotropic half space subjected to surface line loads and distributed loads, respectively. Very few analytical solutions for stresses exist in the literature for half spaces with nonflat surfaces. For a half space of parabolic shape, Kalinin[6] obtained an analytical solution for isotropic media using Muskhelishvili's complex variable method,[7] and Liao and Amadei[8] derived another solution for anisotropic media using Lekhnitskii's analytical function method.[9] More recently Pan and Amadei[10] presented a new analytical method for determining the stress field in a homogeneous, general anisotropic and elastic half space subject to gravity and surface loads under a condition of generalized plane strain and limited by irregular (but smooth) outer boundaries. The stresses were found to depend on three analytical functions that can be determined using a numerical conformal mapping method[11] and an integral equation method.[12]

In this paper the nature of the stress field induced by water reservoir loading of long anisotropic valleys is considered. The rock mass is modeled as a linearly elastic, transversely isotropic or nearly isotropic and homogeneous continuum that deforms under a condition of plane strain. At the outset the new analytical method of Pan and Amadei[10] is reviewed. This method is then used to determine stresses in symmetric and asymmetric valleys induced by water reservoir loading with or without gravity. Numerical examples are presented to analyze the disturbance associated with a water reservoir on the existing gravitational stress field. Finally, a parametric study is presented on the effect of (1) water reservoir height, (2) degree of anisotropy, and (3) orientation of anisotropy on the magnitude and distribution of stresses induced by water reservoir loading only.

Address reprint requests to Dr. Pan at the Department of Civil, Environmental, and Architectural Engineering, University of Colorado at Boulder, Campus Box 428, Boulder, CO 80309-0428.

Received 13 December 1994; revised 7 May 1996; accepted 16 August 1996

655 Avenue of the Americas, New York, NY 10010

0307-904X/96/$15.00
PII S0307-904X(96)00105-4

2. Basic equations

Consider the equilibrium of a half space with the geometry of *Figure 1*. The half space represents a rock mass with an irregular topography that is subject to surface loads (tractions). The medium in the half space is assumed to be linearly elastic, homogeneous, anisotropic, and continuous. An x, y, z coordinate system is attached to the half space, such that the x and z axes are in the horizontal plane and the y axis is pointing upward. We assume that the geometry and elastic properties of the rock mass as well as the surface tractions are independent of the z direction. We also assume that the boundary curve of the half space can be described by an analytic function $y = y(x)$ or in parametric form $x = x(t)$, $y = y(t)$. The half space is subject to the surface tractions t_i $(i = x, y, z)$.

The problem is to find the magnitude and distribution of the stresses induced by the surface loading of the half space. Since the geometry of the problem is independent of the z coordinate and the medium is homogeneous, the stresses can be determined assuming a condition of generalized plane strain, e.g., all planes normal to the z axis are assumed to warp identically.[9] In the absence of body forces, the stresses and strains must satisfy the following equations.[10]

2.1 Equations of equilibrium

$$\frac{\partial \sigma_{xx}}{\partial x} + \frac{\partial \sigma_{xy}}{\partial y} = 0 \tag{1a}$$

$$\frac{\partial \sigma_{xy}}{\partial x} + \frac{\partial \sigma_{yy}}{\partial y} = 0 \tag{1b}$$

$$\frac{\partial \sigma_{xz}}{\partial x} + \frac{\partial \sigma_{yz}}{\partial y} = 0 \tag{1c}$$

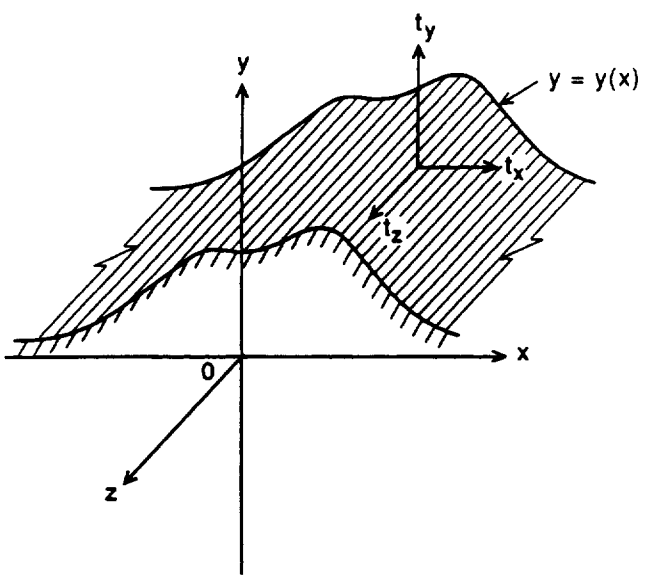

Figure 1. Geometry of the problem. Half space limited by a boundary curve $y=y(x)$, and subject to surface tractions t_i $(i=x,y,z)$.

2.2 Constitutive relations

$$[e] = [a][\sigma] \tag{2}$$

or

$$[\sigma] = [c][e] \tag{3}$$

where

$$[e] = [e_{xx}, e_{yy}, e_{zz}, 2e_{yz}, 2e_{xz}, 2e_{xy}]^T \tag{4}$$

are the strain components, and

$$[\sigma] = [\sigma_{xx}, \sigma_{yy}, \sigma_{zz}, \sigma_{yz}, \sigma_{xz}, \sigma_{xy}]^T \tag{5}$$

are the stress components, $[a]$ is a 6×6 symmetric compliance matrix with 21 independent components a_{ij} $(i, j = 1\text{–}6)$ and $[c]$ is the corresponding stiffness matrix with components c_{ij} $(i, j = 1\text{–}6)$ and is such that $[a] = [c]^{-1}$. In equations (4) and (5), the superscript T indicates the transpose of the matrix. In this paper the rock mechanics sign convention that compressive stresses are positive is adopted.

2.3 Compatibility conditions

$$\frac{\partial e_{xz}}{\partial y} - \frac{\partial e_{yz}}{\partial x} = 0 \tag{6a}$$

$$\frac{\partial^2 e_{xx}}{\partial y^2} + \frac{\partial^2 e_{yy}}{\partial x^2} = 2\frac{\partial^2 e_{xy}}{\partial x\, \partial y} \tag{6b}$$

2.4 Boundary conditions on $y = y(x)$

$$\sigma_{xx}\cos(n, x) + \sigma_{xy}\cos(n, y) = t_x \tag{7a}$$

$$\sigma_{xy}\cos(n, x) + \sigma_{yy}\cos(n, y) = t_y \tag{7b}$$

$$\sigma_{xz}\cos(n, x) + \sigma_{yz}\cos(n, y) = t_z \tag{7c}$$

where $\cos(n, x)$ and $\cos(n, y)$ are the direction cosines of the outward normal, $\mathbf{n}$ of the boundary curve $y = y(x)$.

3. Analytic solutions

Following Lekhnitskii's complex function method,[9] the stress components at each point of the half space in *Figure 1* can be expressed in terms of three analytical functions as follows:

$$\sigma_{xx} = 2\,\mathrm{Re}[\,\mu_1^2\Phi_1'(z_1) + \mu_2^2\Phi_2'(z_2) + \mu_3^2\lambda_3\Phi_3'(z_3)] \tag{8a}$$

$$\sigma_{yy} = 2\,\mathrm{Re}[\Phi_1'(z_1) + \Phi_2'(z_2) + \lambda_3\Phi_3'(z_3)] \tag{8b}$$

$$\sigma_{xy} = -2\,\mathrm{Re}[\mu_1\Phi_1'(z_1) + \mu_2\Phi_2'(z_2) + \mu_3\lambda_3\Phi_3'(z_3)] \tag{8c}$$

$$\sigma_{xz} = 2\,\mathrm{Re}[\mu_1\lambda_1\Phi_1'(z_1) + \mu_2\lambda_2\Phi_2'(z_2) + \mu_3\Phi_3'(z_3)] \tag{8d}$$

$$\sigma_{yz} = -2\,\mathrm{Re}[\lambda_1\Phi_1'(z_1) + \lambda_2\Phi_2'(z_2) + \Phi_3'(z_3)] \tag{8e}$$

$$\sigma_{zz} = -(a_{13}\sigma_{xx} + a_{23}\sigma_{yy} + a_{34}\sigma_{yz} + a_{35}\sigma_{xz} + a_{36}\sigma_{xy})/a_{33} \tag{8f}$$

where μ_1, μ_2, μ_3, λ_1, λ_2, and λ_3 are complex numbers with their values related to the compliance matrix $[a]$. Determination of these complex numbers has been discussed by Lekhnitskii[9] and Pan and Amadei.[10] Also in equations (8a)–(8f), $\Phi_k'(z_k)$ $(k = 1,2,3)$ denote the derivatives of three analytical functions $\Phi_k(z_k)$ with respect to the variable $z_k = x + \mu_k y$, where x and y are the coordinates of the point in the anisotropic medium at which the stresses are calculated. The three functions $\Phi_k(z_k)$ must satisfy the traction conditions along the boundary curve $y = y(x)$, which, in the absence of body forces, can be expressed as follows[10]

$$2\,\mathrm{Re}[\Phi_1(z_1) + \Phi_2(z_2) + \lambda_3\Phi_3(z_3)] = \int_0^s t_y\,ds \tag{9a}$$

$$2\,\mathrm{Re}[\mu_1\Phi_1(z_1) + \mu_2\Phi_2(z_2) + \mu_3\lambda_3\Phi_3(z_3)] = -\int_0^s t_x\,ds \tag{9b}$$

$$2\,\mathrm{Re}[\lambda_1\Phi_1(z_1) + \lambda_2\Phi_2(z_2) + \Phi_3(z_3)] = -\int_0^s t_z\,ds \tag{9c}$$

where s is the arc length along the curve $y = y(x)$.

Determination of the three functions $\Phi_k(z_k)$ and their derivatives depends mainly upon the geometry of the boundary curve $y = y(x)$. As shown by Pan and Amadei,[10] these functions can be determined using a numerical conformal mapping method[11] and an integral equation method.[12] Three new analytical functions Ψ_k $(k = 1,2,3)$ are introduced such that

$$\Psi_k'(\zeta_k) = \Phi_k'(z_k)Z_k'(\zeta_k') \qquad (k = 1,2,3) \tag{10}$$

where the conformal mappings $z_k = Z_k(\zeta_k)$ $(k = 1,2,3)$ that map the lower half planes bounded by $z_k = x(t) + \mu_k y(t)$ onto the lower flat half planes $\mathrm{Im}\,\zeta_k \leqslant 0$ $(k = 1,2,3)$ are obtained by three successive conformal mappings, as discussed in Pan et al.[13] The first (mapping 1), maps the lower half planes bounded by $z_k = x(t) + \mu_k y(t)$ onto irregular bounded domains w_k. The second (mapping 2), maps the irregular bounded domains w_k onto unit disks F_k. Finally, the third (mapping 3) maps the unit disks F_k onto the flat half planes ζ_k. An example of these successive conformal mappings is shown in *Figure 2* where the topography is a symmetric valley. Also in equation (10), $\Psi_k'(\zeta_k)$ and $Z_k'(\zeta_k)$ are the derivatives of Ψ_k and Z_k with respect to ζ_k.

Let t_k be the boundary value of ζ_k. As shown by Pan and Amadei,[10] the boundary conditions (9a)–(9c) lead to the following system of three singular integral equations that can be solved for the three functions $\Psi_k'(t_k)$:

$$b_{11}\Psi_1'(\tau_1) + \frac{b_{12}}{2}\Psi_2'(\tau_2)t_2'(\tau_1) + \frac{b_{13}}{2}\Psi_3'(\tau_3)t_3'(\tau_1) + \frac{b_{12}}{2\pi i}\int_{+\infty}^{-\infty}\frac{\Psi_2'(t_2)t_2'(t_1)\,dt_1}{t_1 - \tau_1} + \frac{b_{13}}{2\pi i}\int_{+\infty}^{-\infty}\frac{\Psi_3'(t_3)t_3'(t_1)\,dt_1}{t_1 - \tau_1} = \frac{f_1(\tau)t'(\tau_1)}{2} + \frac{1}{2\pi i}\int_{+\infty}^{-\infty}\frac{f_1(t)t'(t_1)\,dt_1}{t_1 - \tau_1} \tag{11a}$$

$$b_{21}\Psi_2'(\tau_2) + \frac{b_{22}}{2}\Psi_1'(\tau_1)t_1'(\tau_2) + \frac{b_{23}}{2}\Psi_3'(\tau_3)t_3'(\tau_2) + \frac{b_{22}}{2\pi i}\int_{+\infty}^{-\infty}\frac{\Psi_1'(t_1)t_1'(t_2)\,dt_2}{t_2 - \tau_2} + \frac{b_{23}}{2\pi i}\int_{+\infty}^{-\infty}\frac{\Psi_3'(t_3)t_3'(t_2)\,dt_2}{t_2 - \tau_2} = \frac{f_2(\tau)t'(\tau_2)}{2} + \frac{1}{2\pi i}\int_{+\infty}^{-\infty}\frac{f_2(t)t'(t_2)\,dt_2}{t_2 - \tau_2} \tag{11b}$$

$$b_{31}\Psi_3'(\tau_3) + \frac{b_{32}}{2}\Psi_1'(\tau_1)t_1'(\tau_3) + \frac{b_{33}}{2}\Psi_2'(\tau_2)t_2'(\tau_3) + \frac{b_{32}}{2\pi i}\int_{+\infty}^{-\infty}\frac{\Psi_1'(t_1)t_1'(t_3)\,dt_3}{t_3 - \tau_3} + \frac{b_{33}}{2\pi i}\int_{+\infty}^{-\infty}\frac{\Psi_2'(t_2)t_2'(t_3)\,dt_3}{t_3 - \tau_3} = \frac{f_3(\tau)t'(\tau_3)}{2} + \frac{1}{2\pi i}\int_{+\infty}^{-\infty}\frac{f_3(t)t'(t_3)\,dt_3}{t_3 - \tau_3} \tag{11c}$$

where the coefficients b_{ij} $(i,j = 1,2,3)$ and the functions $f_i(t)$ $(i = 1,2,3)$ are given by equations (25a)–(25i) and equations (26a)–(26c) in the Appendix. In equations (11a)–(11c), τ is a fixed point on the $t[-\infty, +\infty]$ axis and τ_k $(k = 1,2,3)$ are fixed points on the t_k $(\mathrm{Im}\,\zeta_k = 0)$ axes. $t'(t_j)$ and $t_k'(t_j)$ $(k,j = 1,2,3)$ are, respectively, the derivatives of t and t_k with respect to the variable $t_j[-\infty, +\infty]$ and are equal to

$$t'(t_j) = \frac{Z_j'(t_j)}{x'(t) + \mu_j y'(t)} \tag{12a}$$

$$t_k'(t_j) = \frac{Z_j'(t_j)}{Z_k'(t_k)} \cdot \frac{x'(t) + \mu_k y'(t)}{x'(t) + \mu_j y'(t)} \tag{12b}$$

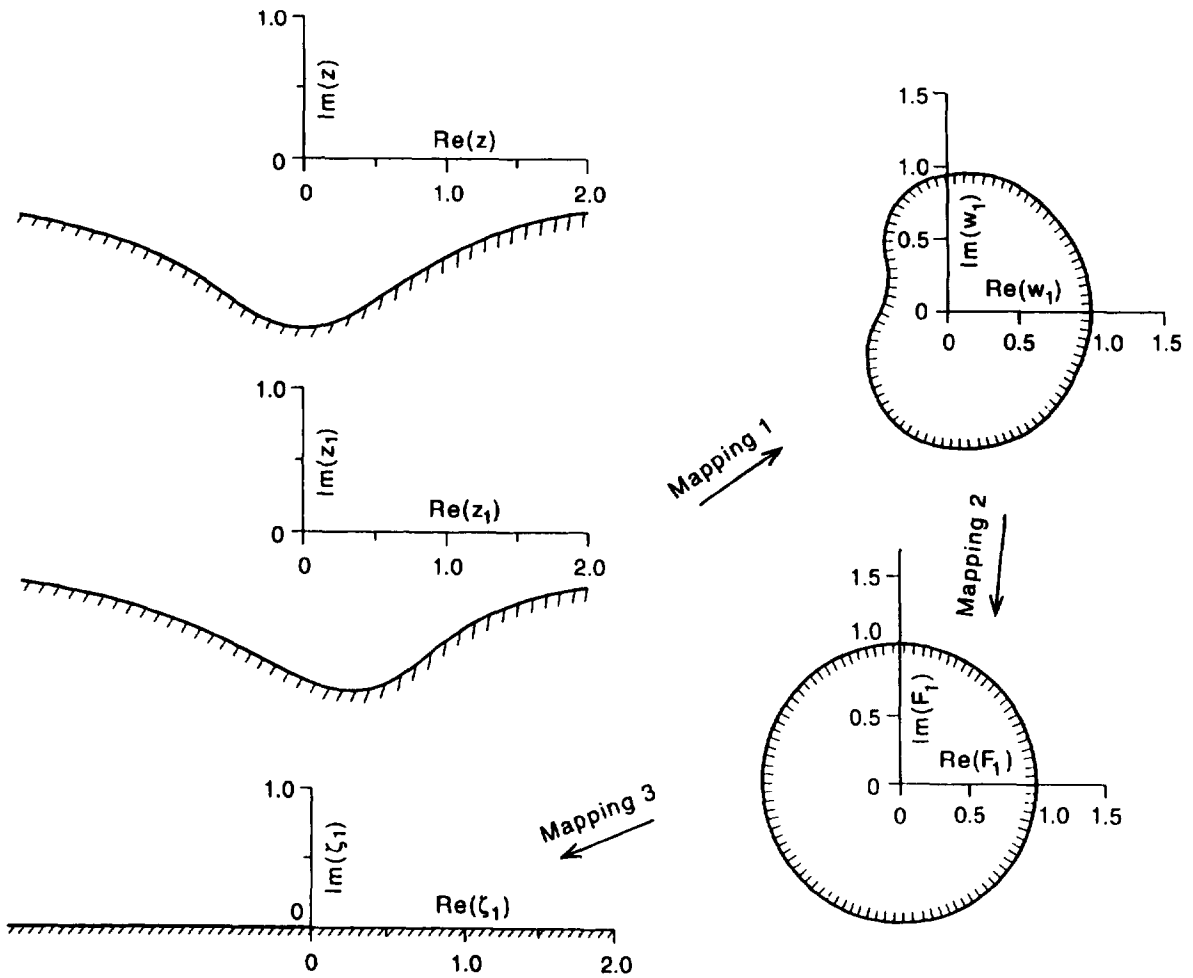

Figure 2. Examples of mappings 1, 2, and 3 for $k=1$ and for the symmetric valley of *Figure 4(a)*. Other parameters are: dip azimuth $\beta=0°$; dip angle $\psi=45°$; and $E/E'=G/G'=3$, $\nu=0.25$, $\nu'=0.15$ (See Ref. 10).

where $x'(t)$ and $y'(t)$ are the derivatives of x and y with respect to t, respectively.

The three integral equations (11a)–(11c) can be discretized and solved for the boundary values of the three analytical functions $\Psi_k'(t_k)$ by the method proposed by Sarkar et al.[14] Then, the interior values of these analytical functions are calculated using the Cauchy integral theorem.[12] Finally, the stress functions $\Phi_k'(z_k)$ are obtained using equation (10), and the six stress components are determined using equations (8a)–(8f). The infinite integrals appearing in equations (11a)–(11c) are determined using an inverse mapping from the boundary of the ζ_k planes to the circumference of unit discs.[10] It is also noted that for these integrals to converge the boundary curve $(x(t), y(t))$ and the surface tractions t_i $(i=x, y, z)$ must be such that the following limits exist:

$$\lim_{t\to\pm\infty} |t_i s'(t)| = a_i < \infty \qquad (i=x,y,z) \tag{13}$$

It is worthy to mention that the proposed method is very accurate and efficient. As shown by Pan and Amedei,[10] the mapping functions $z_k = Z_k(\zeta_k)$ $(k=1,2,3)$ can be determined as accurate as 10^{-15}. When solving the integral equations (11a)–(11c) with 200 discrete points, the stresses can be obtained with an accuracy of 10^{-4}, which is usually better than the series expansion approach.[15]

4. Rock mass elastic properties in local and global coordinate systems

The half space with the geometry of *Figure 1* is assumed to be orthotropic in a local n, s, t cartesian coordinate system attached to planes of anisotropy in the rock mass. The orientation of that local coordinate system with respect to the global x, y, z coordinate system is defined by a dip azimuth β and a dip angle ψ as shown in *Figure 3*. The t-axis is located in the xz plane. The constitutive

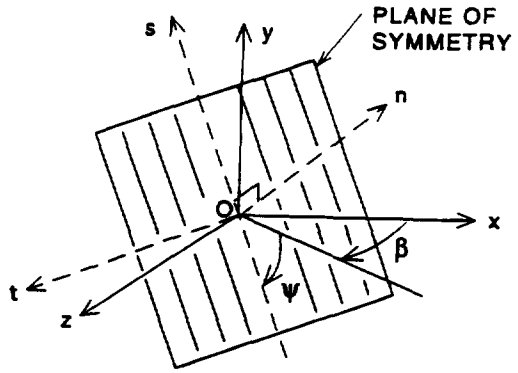

Figure 3. Orientation of planes of symmetry (i.e., the local n,s,t coordinate system) with respect to the global x,y,z coordinate system.

equation in the n,s,t coordinate system is given by the following equation[9]

$$\begin{bmatrix} \epsilon_n \\ \epsilon_s \\ \epsilon_t \\ \gamma_{st} \\ \gamma_{nt} \\ \gamma_{ns} \end{bmatrix} = \begin{vmatrix} \frac{1}{E_n} & -\frac{\nu_{sn}}{E_s} & -\frac{\nu_{tn}}{E_t} & 0 & 0 & 0 \\ -\frac{\nu_{ns}}{E_n} & \frac{1}{E_s} & -\frac{\nu_{ts}}{E_t} & 0 & 0 & 0 \\ -\frac{\nu_{nt}}{E_n} & -\frac{\nu_{st}}{E_s} & \frac{1}{E_t} & 0 & 0 & 0 \\ 0 & 0 & 0 & \frac{1}{G_{st}} & 0 & 0 \\ 0 & 0 & 0 & 0 & \frac{1}{G_{nt}} & 0 \\ 0 & 0 & 0 & 0 & 0 & \frac{1}{G_{ns}} \end{vmatrix} \times \begin{bmatrix} \sigma_{nn} \\ \sigma_{ss} \\ \sigma_{tt} \\ \sigma_{st} \\ \sigma_{nt} \\ \sigma_{ns} \end{bmatrix} \tag{14}$$

or in a more compact matrix form as

$$[e]_{nst} = [h][\sigma]_{nst} \tag{15}$$

In equation (14), E_n, E_s, and E_t are, respectively, the Young's moduli in the n, s, and t directions, respectively. G_{ns}, G_{nt}, and G_{st} are, respectively, the shear moduli in planes parallel to the ns, nt, and st planes, respectively. Finally, ν_{ij} $(i,j=n,s,t)$ are the Poisson's ratios that characterize the normal strains in the symmetry directions j when a stress is applied in the symmetry directions i. Because of symmetry of the compliance matrix $[h]$, Poisson's ratios ν_{ij} and ν_{ji} are such that $\nu_{ij}|E_i = \nu_{ji}|E_j$. Therefore nine independent elastic constants are needed to describe the deformability of the material in the local n,s,t coordinate system.

For known orientations of the planes of anisotropy with respect to the x, y, and z axes, the components of the compliance matrix $[a]$ in equation (2) in the global x,y,z coordinate system can be obtained from those of the compliance matrix $[h]$ in equation (15) by using second-order tensor coordinate transformation rules.[9,16] Because of this linear relationship it can be shown that the stresses in their dimensionless form depend on the following eight dimensionless quantities

$$\frac{E_s}{E_n};\ \frac{E_s}{E_t};\ \nu_{sn};\ \nu_{tn};\ \nu_{ts};\ \frac{E_s}{G_{st}};\ \frac{E_s}{G_{nt}};\ \frac{E_s}{G_{ns}} \tag{16}$$

If the medium in the local n,s,t coordinate system is transversely isotropic in one of the three ns, nt, or st planes, only five independent elastic constants E, E', ν, ν', and G' are needed to describe the deformability of the medium in the n,s,t coordinate system where: (i) E and E' are Young's moduli in the plane of transverse isotropy and in direction normal to it, respectively; (ii) ν and ν' are Poisson's ratios characterizing the lateral strain response in the plane of transverse isotropy to a stress acting parallel and normal to it, respectively; and, (iii) G' is the shear modulus in planes normal to the plane of transverse isotropy. For this case, the stresses in their dimensionless form are found to depend on the following

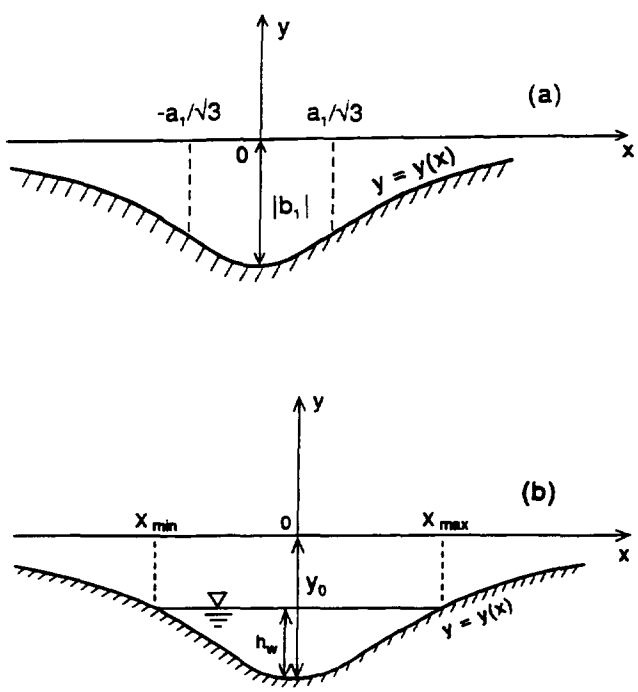

Figure 4. (a) Symmetric valley centered at $x_1=0$ with $a_1/|b_1|=1$. (b) Water reservoir loading. At $x=0$, the water height is equal to h_w and $y_0=|b_1|$.

four dimensionless terms

$$\frac{E}{E'};\ \nu;\ \nu';\ \frac{G}{G'} \tag{17}$$

It is obvious that the stresses in their dimensionless form also depend on (1) the orientation angles β and ψ of the planes of anisotropy with respect to the global x, y, z coordinate system (Fig. 3), (2) the coordinates of the points at which the stresses are calculated, (3) the geometry of the surface topography, and (4) the magnitudes of the surface tractions. Equations (8a)–(8f) show that, in general, at each point in the half space, the stress field is three-dimensional and the principal stress components are inclined with respect to the x, y, and z axes.

The generalized plane strain solution presented above takes a simpler form for orthotropic and transversely isotropic materials with planes of elastic symmetry normal to the z axis of *Figure 1*. This takes place (1) when the dip azimuth β in *Figure 3* is zero and the dip angle ψ varies between 0 and 90 degrees or (2) when the dip azimuth β and the dip angle ψ are both equal to 90 degrees. For those two cases the generalized plane strain solution reduces to a plane strain solution, and the problem of finding the stresses can be decomposed as two uncoupled plane and antiplane problems, which has been discussed in more detail by Pan and Amedei.[10]

5. Water loading of a long valley

The topography of the half space in *Figure 1* is assumed to be smooth and can be expressed in parametric form as follows

$$x(t) = t \qquad (-\infty < t < +\infty) \tag{18a}$$

$$y(t) = \sum_{i=1}^{N} y_i(t) \tag{18b}$$

with

$$y_i(t) = \frac{a_i^2 b_i}{(t - x_i)^2 + a_i^2} \tag{19}$$

Equations (18a), (18b), and (19) correspond to the geometric superposition of $i = 1, N$ symmetric ridges or valleys $x(t), y_i(t)$ centered at $x = x_i$. If b_i is positive, equation (19) corresponds to a ridge with height b_i. If b_i is negative, equation (19) corresponds to a valley with depth $|b_i|$. The parameter a_i controls the lateral extent of each ridge or valley with inflection points located at $x = x_i \pm a_i/\sqrt{3}$, $y = 0.75b_i$ at which the slopes are equal to $\pm 3b_i\sqrt{3}/(8a_i)$.[17] Thus any given smooth topographies can be expressed by choosing different positive or negative values of a_i, b_i, and x_i for $i = 1, N$. As an example, *Figure 4(a)* shows a long isolated symmetric valley with $a_1/|b_1| = 1$ and $x_1 = 0$, and *Figure 5(a)* shows a long asymmetric valley obtained by superposition of two separate symmetric valleys with

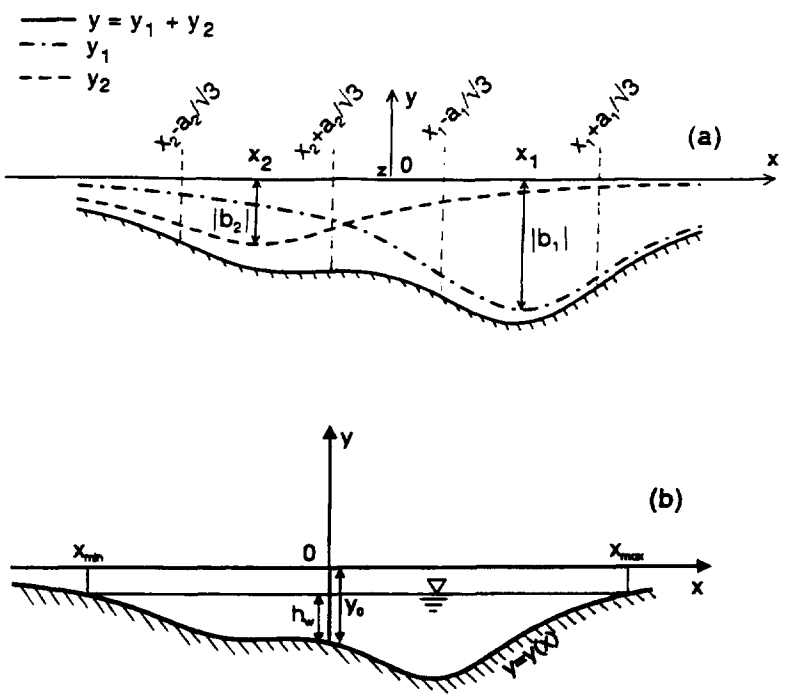

Figure 5. (a) Asymmetric valley obtained by superposition of two separate symmetric valley centered at x_1 and x_2. The parameters are $a_1/|b_1| = a_2/|b_1| = 1$, $x_2/|b_1| = -1$, $b_1/|b_1| = -1$ and $b_2/|b_1| = -0.5$. (b)Water reservoir loading. At $x = 0$, the valley depth is y_0 and the water height is equal to h_w.

$a_1/|b_1| = a_2/|b_1| = -1$, $x_1/|b_1| = 1$, $x_2/|b_1| = -1$, $b_1/|b_1| = -1$, and $b_2/|b_1| = -0.5$.

Consider now the water reservoir loading of a valley with surface topography defined by equations (18a), (18b), and (19). For a given water height $h_w(>0)$ at $x=0$, the water pressure on the valley wall is a function of y only, and can be expressed as

$$p_w = -\rho_w g(y + y_0 - h_w) \tag{20}$$

where $y_0(>0)$ is the depth of the valley at $x=0$, g is the acceleration due to gravity, and ρ_w is the density of water. The water pressure acts over an interval $[x_{min}, x_{max}]$ in the inward normal direction of the boundary curve $y = y(x)$. As an example, *Figures 4(b)* and *5(b)* show the water reservior loading of the valleys of *Figures 4(a)* and *5(a)* respectively.

The surface tractions in the x, y, and z directions corresponding to the water pressure defined in equation (20) are equal to

$$t_x = \frac{-\rho_w g(y + y_0 - h_w)}{s'(t)} \left(2 \sum_{i=1}^{N} \frac{a_i^2 b_i (t - x_i)}{\left[(t - x_i)^2 + a_i^2 \right]^2} \right) \tag{21a}$$

$$t_y = \frac{-\rho_w g(y + y_0 - h_w)}{s'(t)} \tag{21b}$$

$$t_z = 0 \tag{21c}$$

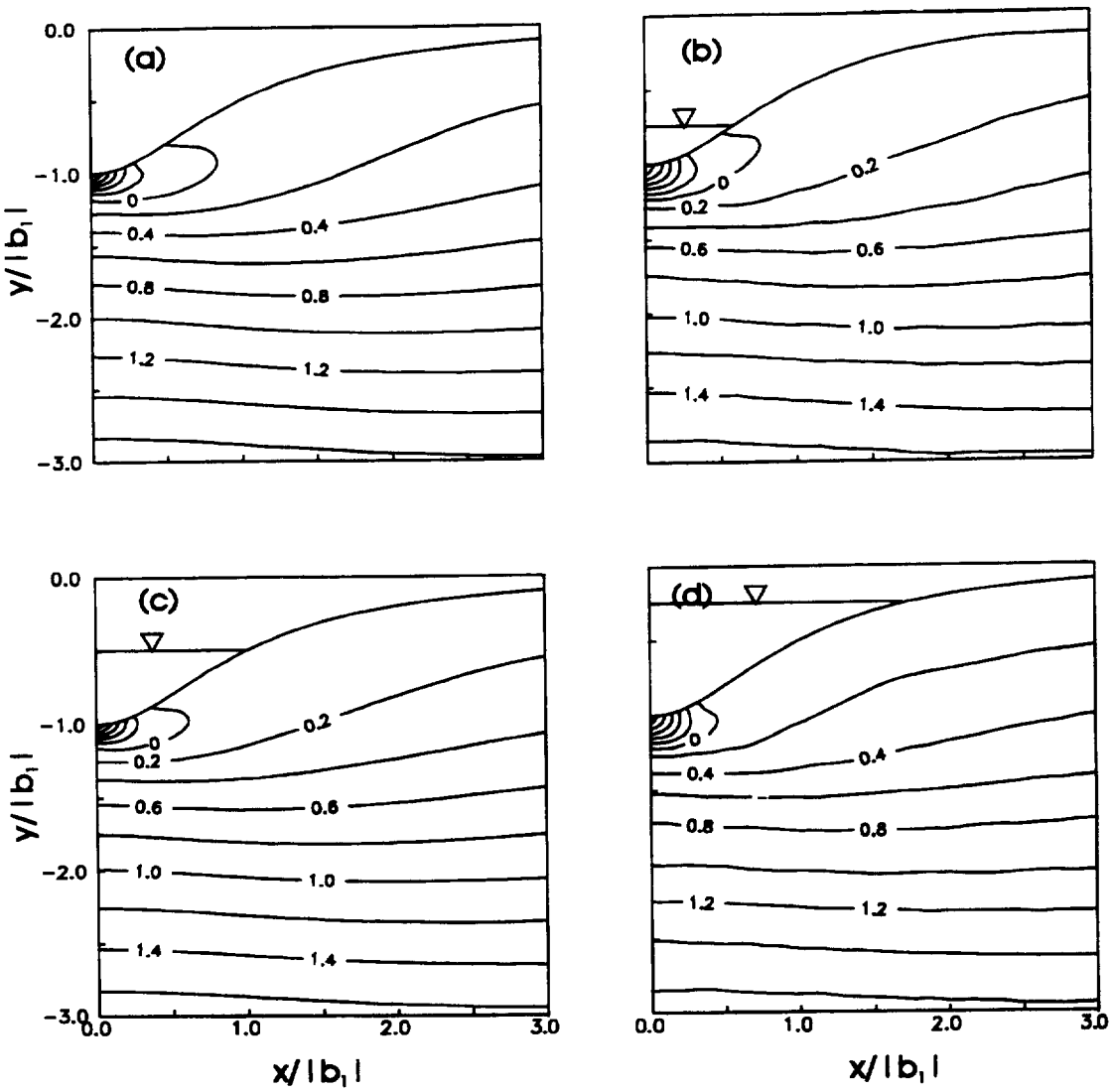

Figure 6. Stress contours of $\sigma_{xx}/\rho g|b_1|$ in a strongly transversely isotropic rock mass ($E/E' = G/G' = 3$, $\nu = 0.25$, $\nu' = 0.15$, and $\psi = 0°$) induced by gravity and water reservoir loading of a symmetric valley with the geometry of *Figure 4(a)*. The density ratio between rock and water $\rho/\rho_w = 2.8$. The normalized water height $h_w/|b_1| = 0$, 0.25, 0.5, and 0.75 in (a), (b), (c), and (d), respectively.

From equations (21a)–(21c), it follows that

$$t_y(t)s'(t) = -\rho_w g(y + y_0 - h_w) \tag{22a}$$

$$t_x(t)s'(t) = -\rho_w g(y + y_0 - h_w) \times \left(2 \sum_{i=1}^{N} \frac{a_i^2 b_i (t - x_i)}{\left[(t - x_i)^2 + a_i^2 \right]^2} \right) \tag{22b}$$

which are two terms entering into the expressions of $f_1(t)$, $f_2(t)$, and $f_3(t)$ in equations (11a)–(11c) and defined in equations (26a)–(26c) in the Appendix. Note that in equations (21a)–(21c) and equations (22a)–(22b), $s'(t)$ is the derivative of the arc length $s(t)$ with respect to the variable t. The latter varies between x_{min} and x_{max}, as the water pressure p_w is nonzero in this interval only. For a given reservoir height h_w, x_{min} and x_{max} are solutions of the following equation

$$y(x) - (h_w - y_0) = 0 \tag{23}$$

6. Numerical examples

To illustrate the theory presented above, numerical examples are presented in *Figures 6–16* on the effect of water reservoir loading on the stress distribution below symmetric and asymmetric valleys with or without gravity. The stress distributions are presented using contour diagrams of dimensionless stresses $\sigma_{xx}/\rho g|b_1|$, $\sigma_{yy}/\rho g|b_1|$ and $\sigma_{xy}/\rho g|b_1|$ where ρ is the rock density and $|b_1|$ is a reference valley depth. When gravity is accounted for, the stresses induced by water reservoir loading are added to the gravitational stresses obtained by Pan et al.[13] and Pan

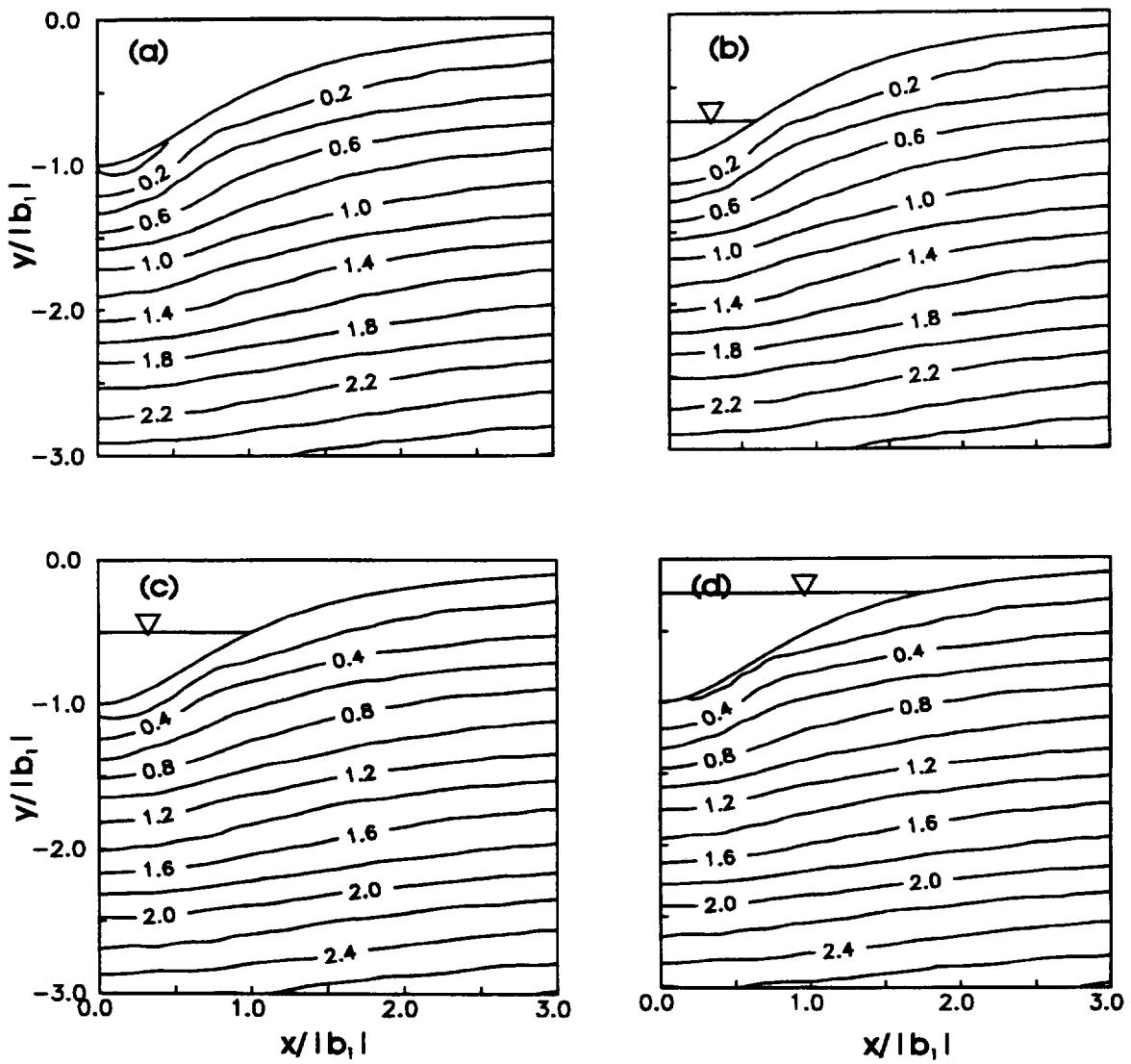

Figure 7. Stress contours of $\sigma_{yy}/\rho g|b_1|$ in a strongly transversely isotropic rock mass ($E/E' = G/G' = 3$, $\nu = 0.25$, $\nu' = 0.15$, and $\psi = 0°$) induced by gravity and water reservoir loading of a symmetric valley with the geometry of *Figure 4(a)*. The density ratio between rock and water $\rho/\rho_w = 2.8$. The normalized water height $h_w/|b_1| = 0$, 0.25, 0.5, and 0.75 in (a), (b), (c), and (d), respectively.

and Amadei.[17] The geometry of *Figure 4(a)* is adopted in the numerical examples show in *Figures 6–14*, and the geometry of *Figure 5(a)* is used in the examples shown in *Figures 15* and *16*. The density ratio between rock and water is taken equal to $\rho/\rho_w = 2.8$. In case of symmetry of the topography as well as of the rock mass properties, only the right halves of the plots of stress contours are presented. The rock mass in the half space is assumed to be either isotropic or transversely isotropic. In the transversely isotropic case, the planes of transverse isotropy are taken parallel to the z-axis ($\beta = 0°$ in *Figure 3*), and the elastic constants are selected within the following restrictions[18]

$$E, E', G, G' > 0 \tag{24a}$$

$$0 \leqslant \nu < 1 \tag{24b}$$

$$1 - \nu - 2\nu'^2 \frac{E}{E'} > 0 \tag{24c}$$

Note that since the anisotropic solution summarized in this paper cannot be reduced directly to the isotropic solution,[10] a nearly isotropic material with $E/E' = G/G' = 1$, $\nu = 0.25$, $\nu' = 0.24$, and $\psi = 0°$ is adopted. Note also that for the orientation of the anisotropy as well as the type of surface loading considered here, the rock mass deforms in plane strain. At each point in the rock mass below the valley, two of the three principal stresses are in the plane normal to the valley axis and the third principal stress is parallel to that axis.

Figures 6, *7*, and *8* show, respectively, contour diagrams of dimensionless stresses $\sigma_{xx}/\rho g|b_1|$, $\sigma_{yy}/\rho g|b_1|$ and $\sigma_{xy}/\rho g|b_1|$ induced by gravity and water reservoir loading of a long symmetric valley with the geometry of *Figure 4(a)*. The rock mass has horizontal planes of transverse

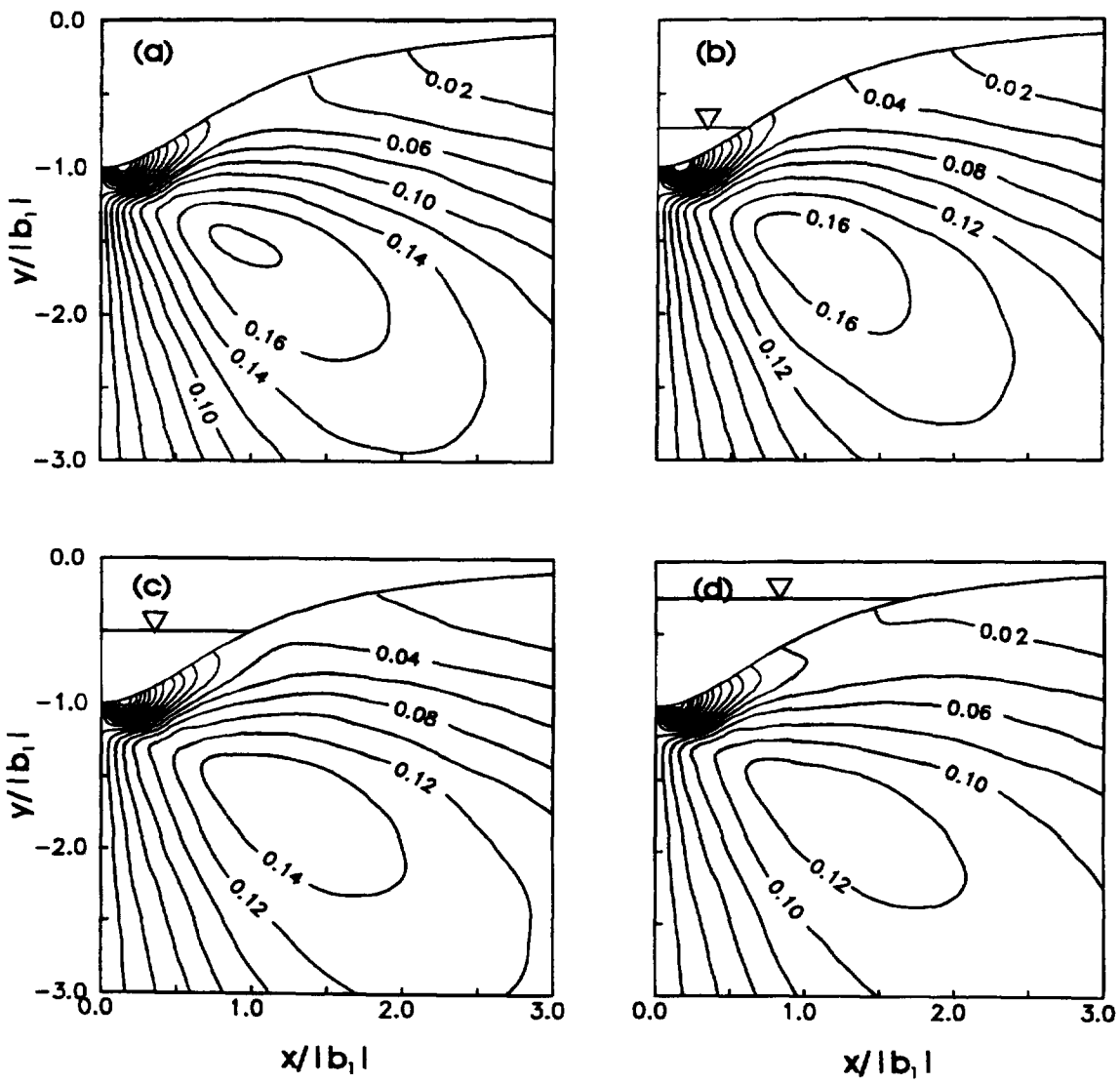

Figure 8. Stress contours of $\sigma_{xy}/\rho g|b_1|$ in a strongly transversely isotropic rock mass ($E/E' = G/G' = 3$, $\nu = 0.25$, $\nu' = 0.15$, and $\psi = 0°$) induced by gravity and water reservoir loading of a symmetric valley with the geometry of *Figure 4(a)*. The density ratio between rock and water $\rho/\rho_w = 2.8$. The normalized water height $h_w/|b_1| = 0$, 0.25, 0.5, and 0.75 in (a), (b), (c), and (d), respectively.

isotropy ($\psi = 0°$) and its elastic properties are such that $E/E' = G/G' = 3$, $\nu = 0.25$, and $\nu' = 0.15$. The normalized water height $h_w/|b_1|$ is equal to 0, 0.25, 0.5, or 0.75. Thus *Figures 6(a)*, *7(a)*, and *8(a)* show respectively, the contours of dimensionless stresses $\sigma_{xx}/\rho g|b_1|$, $\sigma_{yy}/\rho g|b_1|$ and $\sigma_{xy}/\rho g|b_1|$ induced by gravity only.[13] Comparison of *Figure 6(a)* with *6(b)–6(d)* and *Figure 7(a)* with *7(b)–7(d)* indicates that the presence of the water reservoir does not affect much the gravity-induced normal stresses $\sigma_{xx}/\rho g|b_1|$ and $\sigma_{yy}/\rho g|b_1|$, except near the valley bottom. There the effect of the water reservoir is to reduce the magnitude of the gravity-induced horizontal tensile stress (*Figures 6(a)–6(d)*) and to increase the magnitude of the gravity-induced vertical compressive stress (*Figures 7(a)–7(d)*).

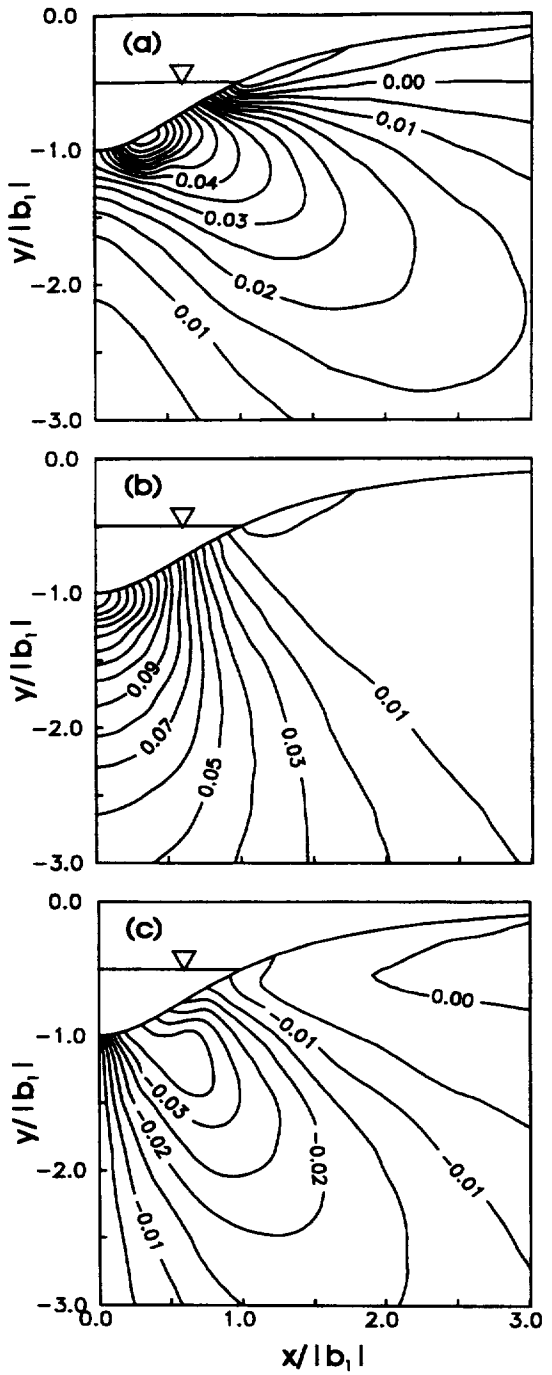

Figure 9. Stress contours of $\sigma_{xx}/\rho g|b_1|$, $\sigma_{yy}/\rho g|b_1|$, and $\sigma_{xy}/\rho g|b_1|$, respectively in (a), (b), and (c), in a nearly isotropic rock mass ($E/E' = G/G' = 1$, $\nu = 0.25$, $\nu' = 0.24$, and $\psi = 0°$) induced by the water reservoir loading only of a symmetric valley with the geometry of *Figure 4(a)*. The normalized water height $h_w/|b_1| = 0.5$ and the density ratio between rock and water $\rho/\rho_w = 2.8$.

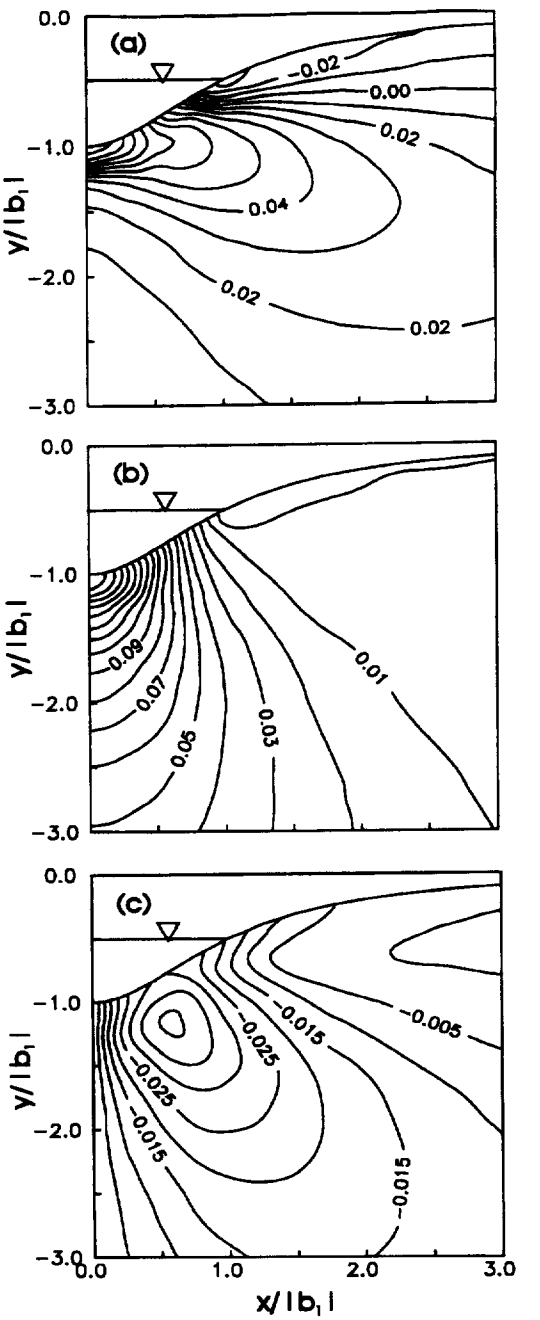

Figure 10. Stress contours of $\sigma_{xx}/\rho g|b_1|$, $\sigma_{yy}/\rho g|b_1|$, and $\sigma_{xy}/\rho g|b_1|$, respectively in (a), (b), and (c), in a strongly transversely isotropic rock mass ($E/E' = G/G' = 3$, $\nu = 0.25$, and $\nu' = 0.15$) induced by the water reservoir loading only. The planes of transverse isotropy are horizontal ($\psi = 0°$). The topography, water height, and density ratio are the same as those in *Figure 9*.

On the other hand comparison of *Figure 8(a)* with *8(b)–8(d)* indicates that the water reservoir affects the gravity-induced shear stress $\sigma_{xy}/\rho g|b_1|$ in a relatively large region below the valley. Water reservoir loading increases the magnitude of the gravity-induced shear stress near the valley bottom and reduces its magnitude elsewhere.

Figures 9–12 show contour diagrams of dimensionless stresses $\sigma_{xx}/\rho g|b_1|$, $\sigma_{yy}/\rho g|b_1|$ and $\sigma_{xy}/\rho g|b_1|$ induced by water reservoir loading only of a symmetric valley with the geometry of *Figure 4(a)*. The water height in the reservoir is fixed and is such that $h_w/|b_1| = 0.5$. The rock is either nearly isotropic or transversely isotropic with horizontal, vertical, or inclined planes of transverse isotropy.

Figures 9(a)–9(c) show contour diagrams of dimensionless stresses in a nearly isotropic rock mass with $E/E' = G/G' = 1$, $\nu = 0.25$, $\nu' = 0.24$, and $\psi = 0°$. A concentration of compressive stress $\sigma_{xx}/\rho g|b_1|$ develops near the valley wall (0.08 at $x/|b_1| = 0.35$ and $y/|b_1| = -0.89$ in *Figure 9(a)*). Also, as expected, the maximum value of $\sigma_{yy}/\rho g|b_1|$ is reached at the valley bottom and is equal to the water pressure at that point (0.18 at $x/|b_1| = 0$ and $y/|b_1| = -1$ in *Figure 9(b)*). For the shear stress $\sigma_{xy}/\rho g|b_1|$, a maxi-

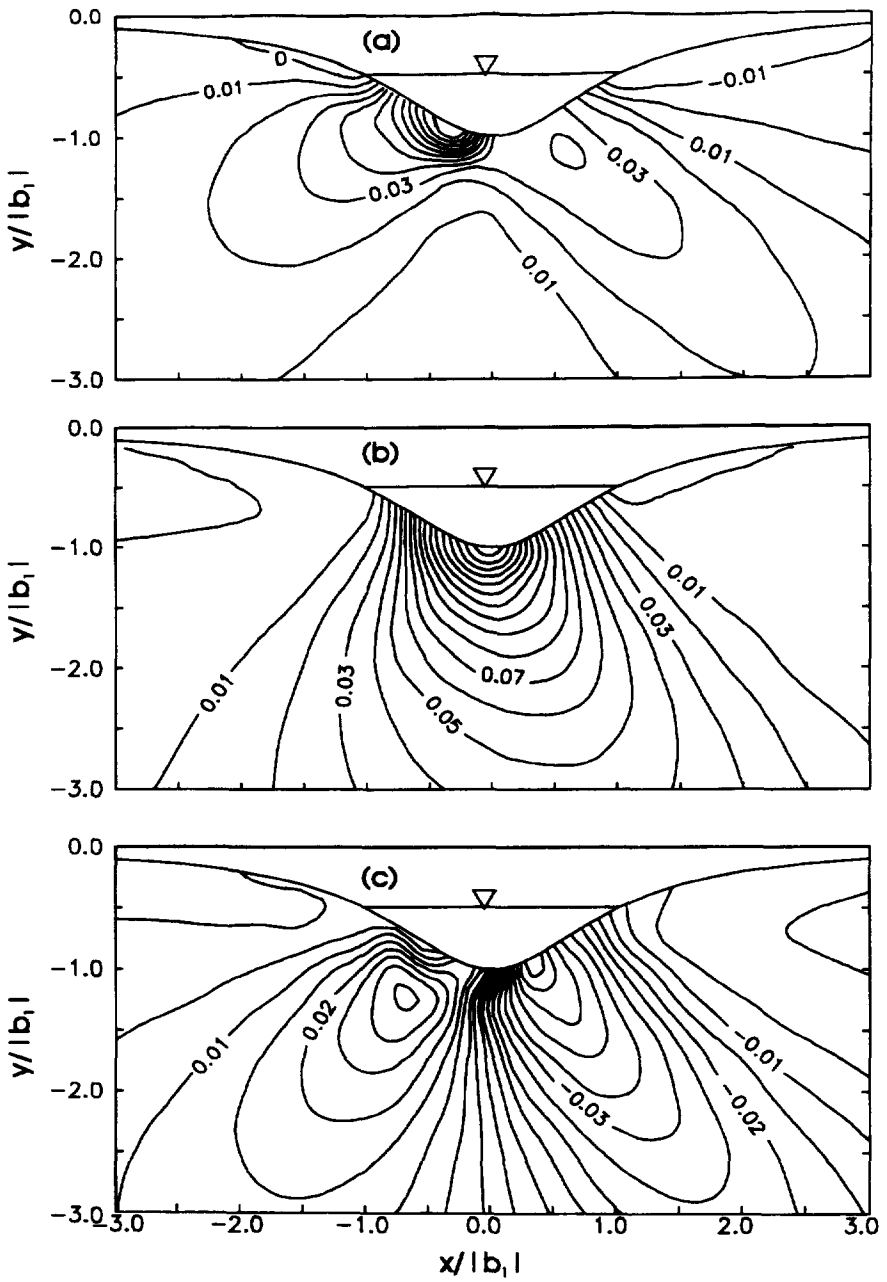

Figure 11. Stress contours of $\sigma_{xx}/\rho g|b_1|$, $\sigma_{yy}/\rho g|b_1|$, and $\sigma_{xy}/\rho g|b_1|$, respectively in (a), (b), and (c), in a strongly transversely isotropic rock mass ($E/E' = G/G' = 3$, $\nu = 0.25$, and $\nu' = 0.15$) induced by the water reservoir loading only. The planes of transverse isotropy are inclined ($\psi = 45°$). The topography, water height, and density ratio are the same as those in *Figure 9*.

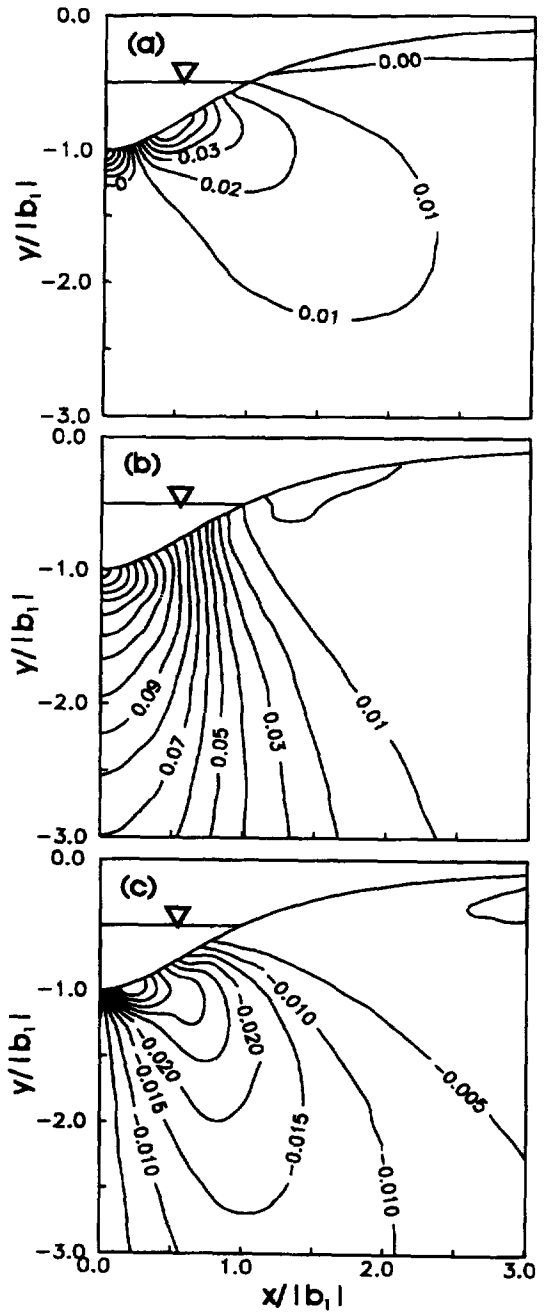

Figure 12. Stress contours of $\sigma_{xx}/\rho g|b_1|$, $\sigma_{yy}/\rho g|b_1|$, and $\sigma_{xy}/\rho g|b_1|$, respectively in (a), (b), and (c), in a strongly transversely isotropic rock mass ($E/E'=G/G'=3$, $\nu=0.25$, and $\nu'=0.15$) induced by the water reservoir loading only. The planes of transverse isotropy are vertical ($\psi=90°$). The topography, water height, and density ratio are the same as those in *Figure 9*.

mum appears at a point below the valley wall (-0.04 at $x/|b_1|=0.5$ and $y/|b_1|=-1.2$ in *Figure 9(c)*). Finally it is interesting to note that for the horizontal stress $\sigma_{xx}/\rho g|b_1|$ a tensile region develops in the valley side starting at the water level (*Figure 9(a)*).

The effect of anisotropy on the contour diagrams of $\sigma_{xx}/\rho g|b_1|$, $\sigma_{yy}/\rho g|b_1|$, and $\sigma_{xy}/\rho g|b_1|$ induced by reservoir loading only of the same valley as in *Figures 9(a)–9(c)* is shown in *Figures 10–12*. The rock is now strongly anisotropic ($E/E'=G/G'=3$, $\nu=0.25$, $\nu'=0.15$) with horizontal ($\psi=0°$), inclined ($\psi=45°$) and vertical ($\psi=90°$) planes of transverse isotropy in *Figures 10*, *11*, and *12*, respectively. Comparison of *Figures 10(a)–10(c)* with *9(a)–9(c)* shows major differences in the $\sigma_{xx}/\rho g|b_1|$ stress contour diagrams. The concentration of compressive stress $\sigma_{xx}/\rho g|b_1|$ is 0.12 at $x/|b_1|=0$ and $y/|b_1|=-1$ (*Figure*

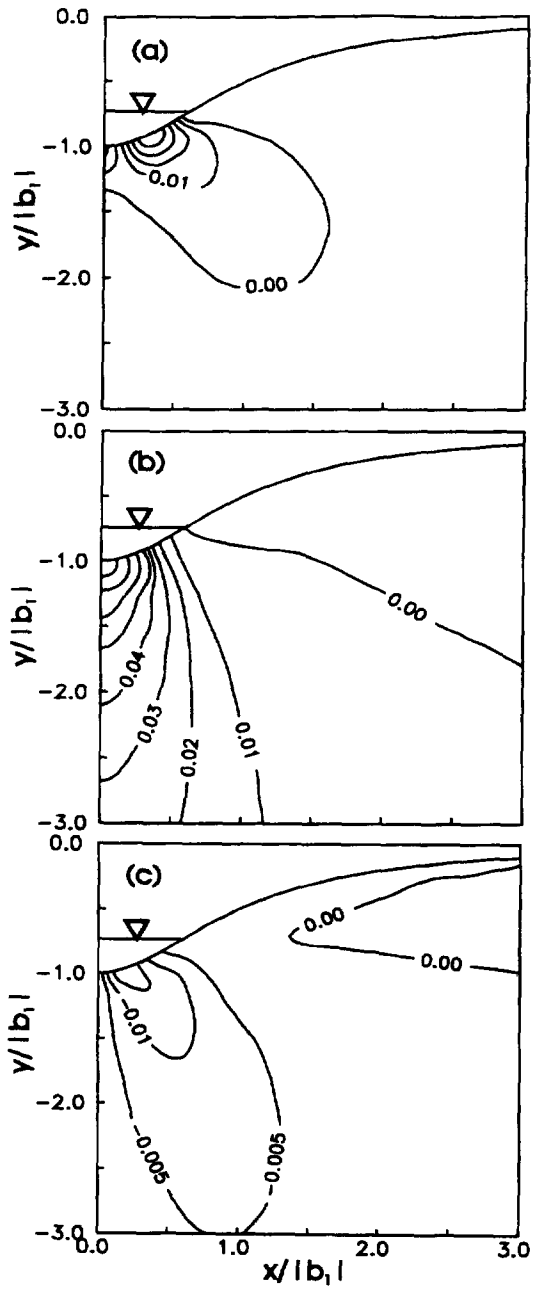

Figure 13. Stress contours of $\sigma_{xx}/\rho g|b_1|$, $\sigma_{yy}/\rho g|b_1|$, and $\sigma_{xy}/\rho g|b_1|$, respectively in (a), (b), and (c), in a strongly transversely isotropic rock mass ($E/E'=G/G'=3$, $\nu=0.25$, $\nu'=0.15$, and $\psi=90°$) induced by the water reservoir loading only of a symmetric valley with the geometry of *Figure 4(a)*. The normalized water height $h_w/|b_1|=0.25$ and the density ratio between rock and water $\rho/\rho_w=2.8$.

10(a)), instead of 0.08 at $x/|b_1| = 0.35$ and $y/|b_1| = -0.89$ for the nearly isotropic case (*Figure 9(a)*). Also more horizontal tension develops in the valley side above the water level for the anisotropic case with a maximum value of $\sigma_{xx}/\rho g|b_1|$ equal to about 0.04 at $x/|b_1| = 1$ and $y/|b_1| = -0.49$ (*Figure 10(a)*), compared to 0.01 at $x/|b_1| = 1.12$ and $y/|b_1| = -0.44$ for the nearly isotropic case (*Figure 9(a)*).

Another interesting feature that can be derived from *Figures 10, 11*, and *12* is the effect of the orientation of the anisotropy on the distribution of stresses induced by water reservoir loading only. At the valley bottom ($x/|b_1| = 0$ and $y/|b_1| = -1$), the horizontal stress $\sigma_{xx}/\rho g|b_1|$ is tensile and equal to -0.06 when the planes of transverse isotropy are vertical (*Figure 12(a)*), but is compressive and equal to 0.12 when the planes of transverse isotropy are horizontal (*Figure 10(a)*). Less tension develops in the valley sides above the water level when the anisotropy is vertical than when it is horizontal. Also the maximum value of $\sigma_{xy}/\rho g|b_1|$ is on the valley wall and equal to -0.05 at $x/|b_1| = 0.21$ and $y/|b_1| = -0.96$ when the anisotropy is vertical (*Figure 12(c)*), instead of being away from the valley walls and equal to -0.04 at $x/|b_1| = 0.6$ and $y/|b_1| = -1.2$ when the anisotropy is horizontal (*Figure 10(c)*). Finally when the planes of transverse isotropy are inclined, the stress distributions are no longer symmetric with respect to the y-axis, as can be seen in *Figure 11(a)–11(c)*. For instance, the horizontal stress $\sigma_{xx}/\rho g|b_1|$ reaches its maximum value on the left-hand wall of the valley (*Figure 11(a)*), instead of at the bottom of the valley

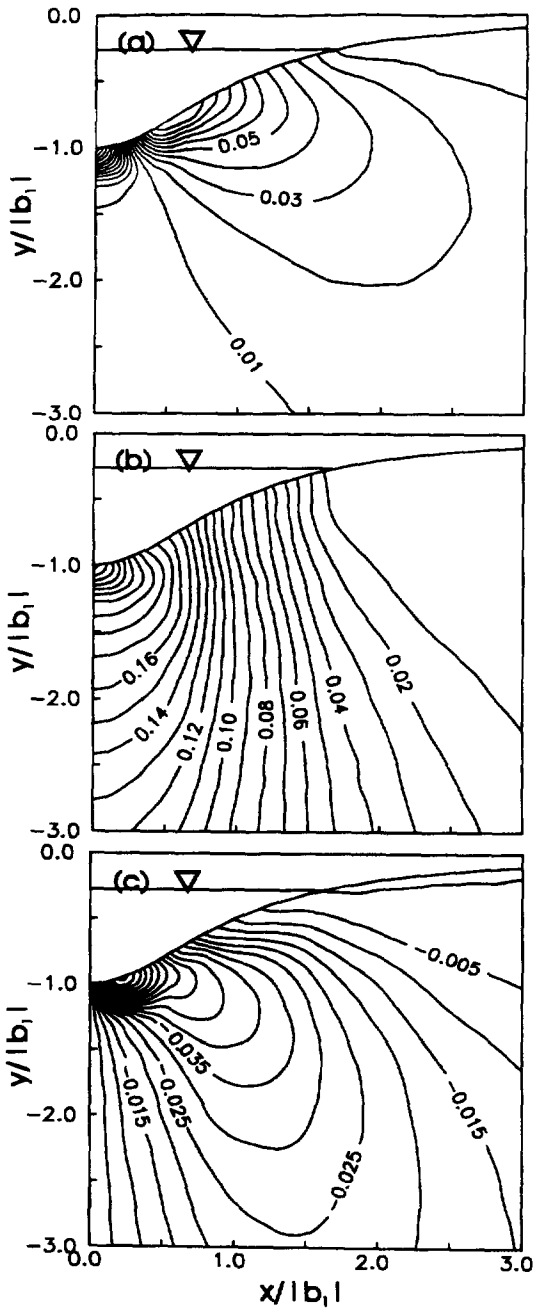

Figure 14. Stress contours of $\sigma_{xx}/\rho g|b_1|$, $\sigma_{yy}/\rho g|b_1|$, and $\sigma_{xy}/\rho g|b_1|$, respectively in (a), (b), and (c), induced by the water reservoir loading with normalized water height $h_w/|b_1| = 0.75$. The topography, elastic properties, and density ratio are the same as those in *Figure 13*.

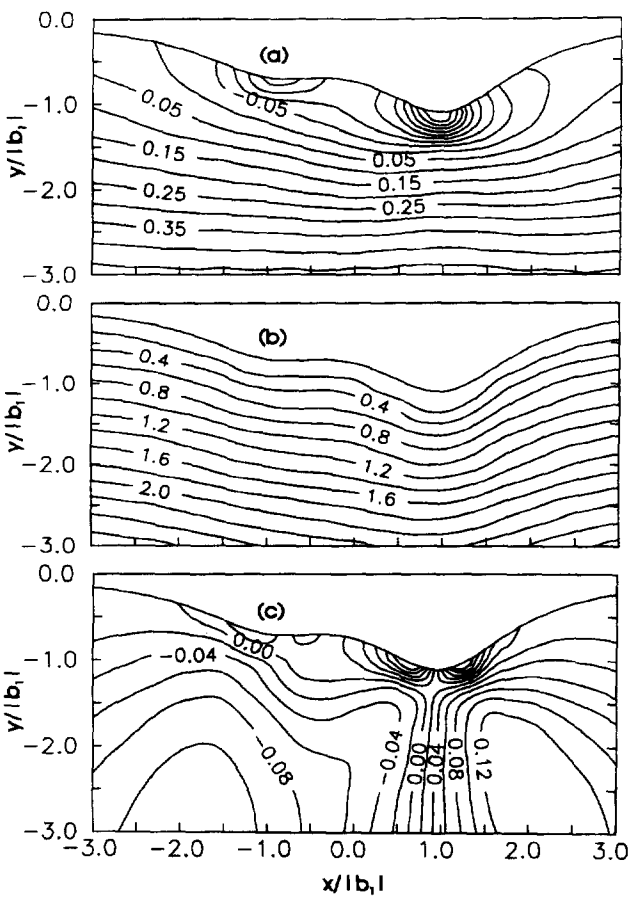

Figure 15. Stress contours of $\sigma_{xx}/\rho g|b_1|$, $\sigma_{yy}/\rho g|b_1|$, and $\sigma_{xy}/\rho g|b_1|$, respectively in (a), (b), and (c), in a strongly transversely isotropic rock mass ($E/E' = G/G' = 3$, $\nu = 0.25$, $\nu' = 0.15$, and $\psi = 90°$) induced by gravitational loading only of an asymmetric valley with the geometry of *Figure 5(a)*.

when the planes of transverse isotropy are horizontal or vertical (*Figures 10(a)* and *12(a)*).

The effect of the water reservoir height on the distribution of dimensionless stresses $\sigma_{xx}/\rho g|b_1|$, $\sigma_{yy}/\rho g|b_1|$ and $\sigma_{xy}/\rho g|b_1|$ induced by water reservoir loading of a symmetric valley with the geometry of *Figure 4(a)* is shown in *Figures 12–14*. The rock mass is transversely isotropic with elastic properties such as $E/E' = G/G' = 3$, $\nu = 0.25$, $\nu' = 0.15$, and it has vertical planes of transverse isotropy. The water height in the reservoir is such that $h_w/|b_1| = 0.25$, 0.5, and 0.75 in *Figures 13*, *12*, and *14*, respectively. These figures indicate that, in general, for a given topography and given rock mass properties, the overall distributions of stress due to water reservoir loading are similar regardless of the water height. At a given point in the rock mass, however, the magnitude of the stresses increases with the water height.

Finally *Figures 15(a)–15(c)* show contour diagrams of dimensionless stresses $\sigma_{xx}/\rho g|b_1|$, $\sigma_{yy}/\rho g|b_1|$, and $\sigma_{xy}/\rho g|b_1|$ induced by gravitational loading only on an asymmetric valley with the geometry of *Figure 5(a)*. For comparison, *Figures 16(a)–16(c)* show the corresponding stress contour diagrams when the valley is subject to both water reservoir loading and gravity with $h_w/|b_1| = 0.5$ at $x = 0$. The rock mass is transversely isotropic with elastic properties such as $E/E' = G/G' = 3$, $\nu = 0.25$, and $\nu' = 0.15$, and it has vertical planes of transverse isotropy. As for the symmetric valley of *Figure 4(a)*, addition of the water reservoir has little effect on the gravity-induced horizontal and vertical normal stresses $\sigma_{xx}/\rho g|b_1|$ and $\sigma_{yy}/\rho g|b_1|$ except near the valley walls, but it affects more the magnitude and distribution of the shear stress $\sigma_{xy}/\rho g|b_1|$.

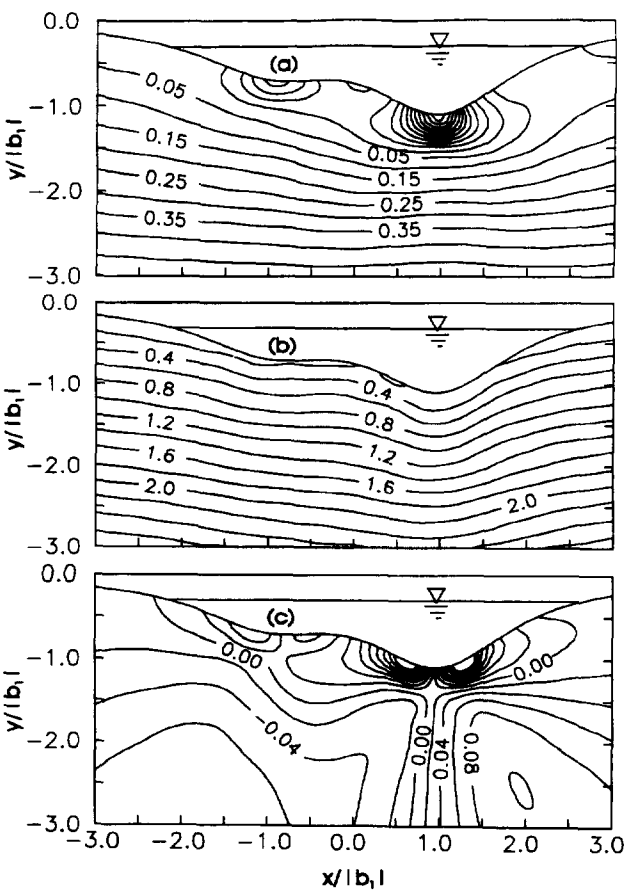

Figure 16. Stress contours of $\sigma_{xx}/\rho g|b_1|$, $\sigma_{yy}/\rho g|b_1|$, and $\sigma_{xy}/\rho g|b_1|$, respectively in (a), (b), and (c), in a strongly transversely isotropic rock mass ($E/E' = G/G' = 3$, $\nu = 0.25$, $\nu' = 0.15$, and $\psi = 90°$) induced by gravity and water reservoir loading of an asymmetric valley with the geometry of *Figure 5(a)*. The normalized water height at $x = 0$ is $h_w/|b_1| = 0.5$, and the density ratio between rock and water $\rho/\rho_w = 2.8$.

7. Conclusions

In this paper the analytical method proposed by Pan and Amadei[10] was used to determine stresses below long valleys in rock masses subject to water reservoir loading. The effect of gravity on the stresses was also taken into account by superposition by using a solution already published by the authors. The method applies to valleys with smooth, symmetric, and asymmetric topographic surfaces of realistic shapes in generally anisotropic, orthotropic, transversely isotropic, or nearly isotropic rock masses. Asymmetric topographic surfaces are obtained by superposition of multiple long and symmetric ridges and valleys.

Water reservoir loading of a long valley (with or without gravity) creates at each point in the rock mass a stress field that is in general three-dimensional. The principal stresses are inclined with respect to the plane normal to the valley axis when the planes of anisotropy are inclined with respect to the valley axis. On the other hand for rock masses with planes of transverse isotropy parallel to or normal to the valley axis, two of the three principal stresses are in the plane normal to that axis and the third principal stress is parallel to that axis.

Numerical examples presented herein indicate that the presence of a water reservoir does not much affect the horizontal and vertical gravity-induced normal stresses except near the valley bottom. There, the effect of the water reservoir is to reduce the magnitude of the gravity-induced horizontal tensile stress and to increase the magnitude of the gravity-induced vertical compressive stress. On the other hand water reservoir loading affects the gravity-induced shear stress in a relatively large region below the valley. Water reservoir loading increases the magnitude of the gravity-induced shear stress near the valley bottom and reduces its magnitude elsewhere.

It was also shown in this paper that under water reservoir loading alone, the stress contours are complicated and depend greatly on the degree and orientation of rock mass anisotropy, as well as the geometry of the topography. For a given topography and given rock mass properties, the overall distributions of stress due to water reservoir loading only are similar regardless of the water height. At a given point in the rock mass, however, the magnitude of the stresses increases with the water height.

The general observations made in this paper may find application in the study of reservoir-induced seismicity[19,20]

which would require knowledge of the effective stress distribution below valleys. Effective stresses can be determined from the total stresses obtained with the analytical method discussed herein and by conducting a seepage analysis of the problem of interest.

Acknowledgment

This research is funded in part by National Science Foundation, Grant No. MS-9215397.

Appendix

Coefficients b_{ij} and functions $f_i(t)$ in equations (11a)–(11c):

$$b_{11} = (\overline{\mu_2} - \mu_1)(\overline{\lambda_2\lambda_3} - 1) - (\overline{\mu_2 - \mu_3})\overline{\lambda_3}(\overline{\lambda_2} - \lambda_1) \tag{25a}$$

$$b_{12} = (\overline{\mu_2} - \mu_2)(\overline{\lambda_2\lambda_3} - 1) - (\overline{\mu_2 - \mu_3})\overline{\lambda_3}(\overline{\lambda_2} - \lambda_2) \tag{25b}$$

$$b_{13} = (\overline{\mu_2} - \mu_3)\lambda_3(\overline{\lambda_2\lambda_3} - 1) - (\overline{\mu_2 - \mu_3})\overline{\lambda_3}(\overline{\lambda_2}\lambda_3 - 1) \tag{25c}$$

$$b_{21} = (\overline{\lambda_1\lambda_3} - 1)(\overline{\mu_1} - \mu_2) - (\overline{\lambda_1} - \lambda_2)\overline{\lambda_3}(\overline{\mu_1 - \mu_3}) \tag{25d}$$

$$b_{22} = (\overline{\lambda_1\lambda_3} - 1)(\overline{\mu_1} - \mu_1) - (\overline{\lambda_1} - \lambda_1)\overline{\lambda_3}(\overline{\mu_1 - \mu_3}) \tag{25e}$$

$$b_{23} = (\overline{\lambda_1\lambda_3} - 1)\lambda_3(\overline{\mu_1} - \mu_3) - (\overline{\lambda_1}\lambda_3 - 1)\overline{\lambda_3}(\overline{\mu_1 - \mu_3}) \tag{25f}$$

$$b_{31} = (\overline{\lambda_1 - \lambda_2})\lambda_3(\overline{\mu_1} - \mu_3) - (\overline{\lambda_1}\lambda_3 - 1)(\overline{\mu_1 - \mu_2}) \tag{25g}$$

$$b_{32} = (\overline{\lambda_1 - \lambda_2})(\overline{\mu_1} - \mu_1) - (\overline{\lambda_1} - \lambda_1)(\overline{\mu_1 - \mu_2}) \tag{25h}$$

$$b_{33} = (\overline{\lambda_1 - \lambda_2})(\overline{\mu_1} - \mu_2) - (\overline{\lambda_1} - \lambda_2)(\overline{\mu_1 - \mu_2}) \tag{25i}$$

$$f_1(t) = [\overline{\mu_2}(\overline{\lambda_2\lambda_3} - 1) - (\overline{\mu_2 - \mu_3})\overline{\lambda_2\lambda_3}]t_y(t)s'(t) + (\overline{\lambda_2\lambda_3} - 1)t_x(t)s'(t) - (\overline{\mu_2 - \mu_3})\overline{\lambda_3}t_z(t)s'(t) \tag{26a}$$

$$f_2(t) = [\overline{\mu_1}(\overline{\lambda_1\lambda_3} - 1) - (\overline{\mu_1 - \mu_3})\overline{\lambda_1\lambda_3}]t_y(t)s'(t) + (\overline{\lambda_1\lambda_3} - 1)t_x(t)s'(t) - (\overline{\mu_1 - \mu_3})\overline{\lambda_3}t_z(t)s'(t) \tag{26b}$$

$$f_3(t) = [\overline{\mu_1}(\overline{\lambda_1 - \lambda_2}) - \overline{\lambda_1}(\overline{\mu_1 - \mu_2})]t_y(t)s'(t) + (\overline{\lambda_1 - \lambda_2})t_x(t)s'(t) - (\overline{\mu_1 - \mu_2})t_z(t)s'(t) \tag{26c}$$

If there is a plane of symmetry normal to the z axis, equations (25) and (26) reduce to

$$b_{11} = \mu_1 - \overline{\mu_2} \tag{27a}$$

$$b_{12} = \mu_2 - \overline{\mu_2} \tag{27b}$$

$$b_{13} = 0 \tag{27c}$$

$$b_{21} = \mu_2 - \overline{\mu_1} \tag{27d}$$

$$b_{22} = \mu_1 - \overline{\mu_1} \tag{27e}$$

$$b_{23} = 0 \tag{27f}$$

$$b_{31} = \overline{\mu_1 - \mu_2} \tag{27g}$$

$$b_{32} = 0 \tag{27h}$$

$$b_{33} = 0 \tag{27i}$$

and

$$f_1(t) = -\overline{\mu_2}t_y(t)s'(t) - t_x(t)s'(t) \tag{28a}$$

$$f_2(t) = -\overline{\mu_1}t_y(t)s'(t) - t_x(t)s'(t) \tag{28b}$$

$$f_3(t) = -(\overline{\mu_1 - \mu_2})t_z(t)s'(t) \tag{28c}$$

References

1. Timoshenko, S. P. and Goodier, J. N. *Theory of elasticity* (3rd ed.) McGraw-Hill, New York, 1970
2. Conway, H. D. and Ithaca, N. Y. Some problems of orthotropic plane stress, *J. Appl. Mech.* 1953, **75**, 72–76
3. Conway, H. D. and Ithaca, N. Y. Note on orthotropic half space subjected to concentrated loads, *J. Appl. Mech.* 1955, **77**, 130
4. Urena, R. D., Piquer, J. S., Muzas, F., and Saracho, J. M. S. Stress distribution in cross-anisotropic media, *Proceedings of the 1st Congress of the International Society of Rock Mechanics*, 1966, Volume **1**, pp. 313–317
5. Piquer, J. S., Muzas, F, Urena, R. D. and Grajera, F. Foundations in cross-anisotropic ground, *Proceedings of the 1st Congress of the International Society of Rock Mechanics*, 1966, Volume **2**, pp. 531–536
6. Kalinin, E. V. The change in the stressed state of a rock massif at the base of a storage lake, *Problems of the Forming and Stability of High Slopes*, Moscow State University Press, Moscow, 1970, pp. 97–104
7. Muskhelishvili, N. I. *Some Basic Problems of the Mathematical Theory of Elasticity*. Noordhoff, Groningen, The Netherlands, 1953
8. Liao, J. J. and Amadei, B. Surface loading of anisotropic rock masses, *J. Geotech. Engrg.* 1991, **11**, 1779–1800
9. Lekhnitskii, S. G. *Theory of elasticity of an anisotropic elastic body*. Holden-Day, San Francisco, 1963
10. Pan, E. and Amadei, B. Stresses in anisotropic rock mass with irregular topography. *J. Eng. Mech.* 1994, **120**, 97–119
11. Trummer, M. R. An efficient implementation of a conformal mapping method based on the Szegö kernel. *J. Numer. Anal.* 1986, **23**, 853–872
12. Muskhelishvili, N. I. *Singular integral equations*. Noordhoff, Groningen, The Netherlands, 1972
13. Pan, E., Amadei, B., and Savage, W. Z. Gravitational stresses in long symmetric ridges and valleys in anisotropic rock. *Int. J. Rock Mech. Min. Sci. & Geomech. Abstr.* 1994, **31**, 293–312

14. Sarkar, T. K., Yang, X., and Arvas, E. A limited survey of various conjugate gradient methods for solving complex matrix equations arising in electromagnetic wave interactions. *Wave Motion* 1988, **10**, 527–546
15. Verruijt, A. Stresses due to gravity in a notched elastic half-plane. *Ingenieur-Archiv* 1969, **38**, 107–118
16. Amadei, B. *Rock Anisotropy and the Theory of Stress Measurements*. Springer-Verlag, New York, 1983
17. Pan, E. and Amadei, B. Gravitational stresses in long asymmetric ridges and valleys. *Int. J. Rock Mech. Min. Sci. Geomech. Abstr.* 1993, **30**, 1005–1008
18. Lempriere, B. M. Poisson's ratios in orthotropic materials. *J. Am. Inst. Aeronaut. Astronaut.* 1968, **6**, 2226–2227
19. Kisslinger, C. A review of theories of mechanisms of induced seismicity. *Eng. Geol.* 1976, **10**, 85–98
20. Simpson, D. W. Seismicity changes associated with reservoir loading. *Eng. Geol.* 1976, **10**, 123–150